Recovery of Uniform Samples and Spectrum of Band-limited Irregularly Sampled Signals

Ghazaei, Mahdi; Johansson, Rolf

2016

Document Version:
Publisher's PDF, also known as Version of record

ISSN 0280–5316
ISRN LUTFD2/TFRT--7647--SE

Recovery of Uniform Samples and Spectrum of Band-limited Irregularly Sampled Signals

M. Mahdi Ghazaei Ardakani
Rolf Johansson

Department of Automatic Control
Lund Institute of Technology
June 2016

Abstract

This paper presents a straightforward method to convert non-uniformly sampled data to uniform samples in order to be processed by some off-line techniques such as system identification. In such scenarios, we deal with a finite-length measurement sequence. We assume periodic extension of the signals, which results in a simple system of linear equations. Furthermore, we take into account a number of practical considerations for solving the system of equations and dealing with issues such as loss of samples. Thanks to the insights from the frequency domain, a non-integer delay element with respect to discrete-time signals is introduced. This interpretation leads to iterative algorithms for reconstruction of either time or frequency representations of the non-uniform samples. We provide simulation results for the case of jitter in the sampling clock and/or drops. Finally, our approach is compared with a few earlier works and the results are discussed.

Index Terms

non-uniform sampling, interpolation, spectral analysis, iterative methods, non-integer delay.

I. Introduction

CURRENT techniques for analysis and processing of digital signals are mainly developed for the case of uniform sampling [1]. This applies to both off-line techniques, e.g., spectral analysis and system identification, and on-line processing, such as filtering and control applications. Although non-uniform sampling may prove useful in some applications [2]–[4], usually unplanned variations or jitter in sampling instants are considered troublesome.

Today's control applications typically have elements such as computer networks or radio links. Therefore, in addition to an unstable clock, we might experience data drops and variable delays. In such scenarios, we encounter difficulties to apply common system identification techniques. A natural solution could be transforming the non-uniform samples to uniform samples. This problem can be treated as an interpolation task where the missing data is to be estimated.

For interpolation, piece-wise linear or cubic spline approaches are commonly used. The former provides an easy and quick way to evaluate values at the missing data points and the latter is popular because it can approximate complex curves. Spline of order n calculates piecewise-polynomial functions that pass through all the existing data and is continuously differentiable up to the order of $n-1$ at these points [5]. While these methods try to smoothly interpolate data, they are not able to incorporate some global information. Therefore, they fail to extrapolate beyond the input interval or give a reasonable response where a number of samples are missing. More importantly, to faithfully reconstruct a band-limited signal by a spline, an infinite order spline would be required [6].

Recovering of a band-limited signal from its non-uniform samples has a long history. The connection between band-limited functions and entire functions of exponential type has made it possible to reuse many earlier results in this context. In particular, the results by Paley-Wiener [7] and Kadec [8] on nonharmonic Fourier bases can be directly applied in this area. The celebrated theorem due to the work of Beurling [9] and Landau [10] has provided a necessary and sufficient condition for the sampling density for stable reconstruction. The frame theory due to Duffin-Schaeffer [11] is another influential work, which has laid the theoretical ground for many iterative algorithms.

In the classic work by Yen [12], various schemes of deviation from a uniform grid have been considered. Explicit formulae for recovering a signal from such perturbed grids has been proposed. Specifically, in the fourth theorem of this work, the concept of minimum-energy signals has been introduced, which allows to uniquely reconstruct a band-limited signal from a finite set of arbitrarily distributed samples.

There are many iterative methods based on the well-known inversion of a linear operator by means of Neumann series, which reduce to Richardson's method [13, p. 22]. Among others, it has been shown that by successively applying a combination of band-limiting and sampling operations, the original signal is recoverable for different types of sampling methods, e.g., sample and hold and natural sampling [14]. Further results concerning the convergence of this method and a comprehensive reference to the field can be found in [15].

A direct treatment of the discrete problem of irregular sampling with focus on iterative methods has been given in [16]. In addition, the author has discussed a closely related problem of interpolation of trigonometric polynomials. In [17], an efficient frame based algorithm has been proposed. The main ingredients of their approach are conjugate gradient method instead of Richardson's, preconditioning of data by adaptive weights, and utilizing Toeplitz structure of the system matrix. It has been shown that a certain trigonometric polynomial fitted to the data converges to the solution of an infinite-dimensional reconstruction problem [18]. To motivate the proposed iterative algorithm, a uniform estimate of the condition number of the reconstruction operator based on the maximum gap between samples has been given. The earlier approaches have been nicely brought together and presented in a unified framework for reconstructing a broader class of shift-invariant functions in [19].

Projection Onto Convex Sets (POCS) [20] and its variants [21] offer an alternative way for reconstructing signals than frame based iterative algorithms. The idea is projecting an initial function sequentially to a set of convex sets, each containing all of the functions coinciding at a sample with the function to be reconstructed. Since, this iterative algorithm suffers from a slow convergence rate, a one-step formulation has also been proposed. In a general case, the one-step formulation requires the inversion of an unstructured matrix whose size grows with the number of samples.

A direct approach for reconstruction of the digital spectrum of non-uniformly sampled signal with periodic sampling structure has been suggested in [22]. A spectrum with a desired resolution has been obtained by solving a system of linear equations. In [23], it has been assumed that non-uniform samples lie on a fine grid. Accordingly, a linear system of equations has been formed and solved for uniform samples. The drawback of the method is that the performance decreases as the resolution of the non-uniform grid increases. In another work, the more specific case of periodic and band-limited signals has been considered [24]. The authors provide explicit formulae for reconstruction from even or odd number of non-uniform samples.

In this article, the reconstruction of bandwidth-limited one-dimensional signals from time-stamped non-uniformly sampled data is investigated. Specifically, we would like to find the equally-spaced samples and the spectrum of a band-limited signal that coincides with the samples taken at known sampling instants. We introduce a novel view point based on the periodic extension as well as new algorithms. Our sampling model is compatible with any arbitrary sampling scheme.

Therefore, we make no implicit assumption regarding the sampling pattern in advance. We provide an explicit formula for the Inverse Discrete Fourier Transform (IDFT) of non-uniformly sampled data and present an efficient way to compute their Discrete Fourier Transform (DFT). The basis functions for uniform periodic signals cover both even and odd number of samples. For recovering uniform samples and spectrum, we propose two approaches; one-stage and iterative. The one-stage method allows trade-off between accuracy and other smoothness criteria and our batch-mode iterative algorithm offers more favorable convergence properties than the generic Jacobi method [13].

The remainder of the paper is organized as follows. In Section II, we make a reformulation of the Nyquist ideal reconstruction for periodic signals. Subsequently, Section III deals with one-stage approach to estimate uniform samples. In Section IV, we revisit the properties of our interpolation basis in the frequency domain. This leads to the definition of a non-integer forward shift element. Consequently, we develop iterative algorithms under the light of this interpretation. Section V presents simulation results for both approaches under various conditions. We discuss the results and link our approaches to some of the earlier works by pointing out similarities and differences in Section VI. Section VII presents our conclusions.

II. Model of Non-uniformly Sampled Data

It is well known that a band-limited signal can be ideally reconstructed if it is uniformly sampled at a rate not less than the Nyquist rate. Otherwise, without any prior information, aliasing effect can distort the frequency content of the signal beyond recovery [25], [26]. Fortunately, most practical systems have a limited bandwidth. This is especially true for a closed-loop system, where good robustness and measurement noise rejection are achieved by limiting the high-frequency content of the control loop [27].

Assuming the conditions of the Nyquist theorem hold, according to the Whittaker–Shannon interpolation formula, we can calculate the original signal from its samples by [25], [28]

$$y(t) = \sum_{k=-\infty}^{\infty} y(kT_s) \cdot \operatorname{sinc}\left(\frac{t - kT_s}{T_s}\right), \tag{1}$$

where $\operatorname{sinc}(x) = \sin(\pi x)/\pi x$ and $T_s \in \mathbb{R}$ is the sampling period. This is in fact an interpolation of uniform samples with $\operatorname{sinc}\left(t/T_s - k\right)$ as an orthogonal basis which can perfectly evaluate a signal at any time instant.

Since we deal with a finite measurement interval, we are only interested in a finite number of uniform samples covering the measurement period. However, the recovery of a sample according to (1) requires the knowledge of all the uniform samples. To address this problem, we assume periodic extension of $y[k]$ beyond the measurement window. This means that we project the signals into the space of band-limited and periodic signals. Let us denote this space by $\mathcal{B}_N$ where N is the number of the samples. According to [29], [30], this space can be expanded by the following bases:

$$\operatorname{psinc}_N(x) \equiv \begin{cases} \dfrac{\sin \pi x}{N \sin \frac{\pi}{N} x} & N \text{ odd} \\ \dfrac{\sin \pi x}{N \tan \frac{\pi}{N} x} & N \text{ even.} \end{cases} \tag{2}$$

Note that the function defined above is periodic with period of N. Moreover,

$$\lim_{N\to\infty} \mathrm{psinc}_N(x) = \mathrm{sinc}\,(x)\,. \tag{3}$$

Given (2), we can express the signals in the space of $\mathcal{B}_N$ by

$$y(t) = \sum_{k=0}^{N-1} y[k] \cdot \mathrm{psinc}_N\left(\frac{t}{T_s} - k\right), \tag{4}$$

where we have defined $y[k] \equiv y(kT_s)$.

Assume that we have a set of distinct measurements at

$$\{t_n = nT_s + \tau_n T_s : n \in \{0,\ldots,N-1\} \wedge \tau_n \in \mathbb{R}\}\,. \tag{5}$$

By substituting the expression for t_n into (4) and denoting the estimates of the actual $y[k]$ by $\tilde{y}[k]$, we obtain

$$y(t_n) = \sum_{k=0}^{N-1} \tilde{y}[k] \cdot \mathrm{psinc}_N^{\tau_n}\,[n-k]\,, \tag{6}$$

where we have introduced the following notation

$$\mathrm{psinc}_N^{\tau}[n] \equiv \mathrm{psinc}_N(n+\tau). \tag{7}$$

Note that τ is unitless and describes the amount of deviation from a uniform grid in proportion to the sampling period T_s.

According to (6), every $y(t_n)$ imposes an affine constraint on the underlying uniform samples $\tilde{y}[k]$. These constraints can be conveniently arranged in a square matrix to be solved for $\tilde{y}[k]$:

$$\mathbf{y} = \mathbf{A}\tilde{\mathbf{y}} \tag{8}$$

$$A_{\ell,k} = \mathrm{psinc}_N^{\tau_\ell}\,[\ell - k]\,, \qquad 0 \le l,k < N. \tag{9}$$

Theorem 1: The matrix $\mathbf{A} \in \mathbb{R}^{N\times N}$ defined in (9) can be factorized as

$$\mathbf{A} = \mathbf{W}\mathbf{V}, \tag{10}$$

where $\mathbf{W}$, $\mathbf{V} \in \mathbb{R}^{N\times N}$. If N is odd,

$$\mathbf{W} = \frac{1}{N}\begin{pmatrix} 1 & \cdots & w_0^{\lfloor\frac{N-1}{2}\rfloor} & w_0^{-\lfloor\frac{N-1}{2}\rfloor} & \cdots & w_0^{-1} \\ 1 & \cdots & w_1^{\lfloor\frac{N-1}{2}\rfloor} & w_1^{-\lfloor\frac{N-1}{2}\rfloor} & \cdots & w_1^{-1} \\ \vdots & \ddots & \vdots & \vdots & \ddots & \vdots \\ 1 & \cdots & w_{N-1}^{\lfloor\frac{N-1}{2}\rfloor} & w_{N-1}^{-\lfloor\frac{N-1}{2}\rfloor} & \cdots & w_{N-1}^{-1} \end{pmatrix} \tag{11}$$

where $w_n = \mathrm{e}^{i2\pi(n+\tau_n)/N}$. For an even N, the matrix description is similar, but an additional column should be inserted in the middle of the matrix. Namely, $(N/2+1)$-th column will be

$$\mathbf{W}_{N/2} = \begin{pmatrix} \frac{1}{2}(w_0^{N/2} + w_0^{-N/2}) \\ \frac{1}{2}(w_1^{N/2} + w_1^{-N/2}) \\ \vdots \\ \frac{1}{2}(w_{N-1}^{N/2} + w_{N-1}^{-N/2}) \end{pmatrix}. \tag{12}$$

The matrix $\mathbf{V}$ is the Discrete Fourier Transform (DFT) expressed as a Vandermonde matrix,

$$\mathbf{V} = \begin{pmatrix} 1 & v_0^1 & \cdots & v_0^{N-1} \\ 1 & v_1^1 & \cdots & v_1^{N-1} \\ \vdots & \vdots & \ddots & \vdots \\ 1 & v_{N-1}^1 & \cdots & v_{N-1}^{N-1} \end{pmatrix}, \; v_n = \mathrm{e}^{-i\frac{2\pi}{N}n}. \tag{13}$$

Proof: Note that

$$\mathrm{psinc}_N^{\tau}[n] = \begin{cases} \dfrac{1}{N} \displaystyle\sum_{k=-\lfloor\frac{N-1}{2}\rfloor}^{\lfloor\frac{N-1}{2}\rfloor} \mathrm{e}^{i2\pi\frac{k}{N}(n+\tau)} & N \text{ odd} \\ \dfrac{1}{N} \displaystyle\sum_{k=-\lfloor\frac{N-1}{2}\rfloor}^{\lfloor\frac{N-1}{2}\rfloor} \mathrm{e}^{i2\pi\frac{k}{N}(n+\tau)} & N \text{ even} \\ \quad + \dfrac{1}{2N}\left(\mathrm{e}^{-i\pi(n+\tau)} + \mathrm{e}^{i\pi(n+\tau)}\right) & \end{cases} \tag{14}$$

The proof follows directly from (9) and the definitions of $\mathbf{W}$ and $\mathbf{V}$. ■

Remark 1: Theorem 1 provides an important interpretation for matrix $\mathbf{W}$, which is the IDFT of the non-uniform samples. Note the similarity between this matrix and the uniform IDFT where τ_n equals to zero for all n. In view of this, we write

$$\mathbf{y} = \mathbf{W}\tilde{\mathbf{Y}}, \tag{15}$$

where $\tilde{\mathbf{Y}}$ denotes the DFT of $\tilde{\mathbf{y}}$.

Theorem 2: The matrix $\mathbf{A}$ defined in (9) has full rank provided that there are N distinct measurement points. If N is even, it is additionally required that for all $k \in \mathbb{Z}$ $\sum_{n=0}^{N-1} \tau_n \neq (2k+1)N/2$.

Proof: See Appendix A. ■

Corollary 1: If $|\tau_n| < 1/2$, $\forall n$, then matrix $\mathbf{A}$ has full rank.

Based on the relations in this section, we develop two approaches in the next two sections to solve for $\tilde{y}[k]$ given $y(t_n)$ values.

III. One-stage Approach

The matrix $\mathbf{A}$ projects uniform samples to non-uniform samples according to a prescribed sampling scheme. Theorem 2 ensures that matrices $\mathbf{A}$ and $\mathbf{W}$ are invertible, hence we can solve for uniform samples and the spectrum using (8) and (15), respectively. Note that solving (15) amounts to calculating the DFT of the non-uniform samples. Although it is possible to find an explicit and fairly compact formula for non-uniform DFT exploiting the Vandermonde structures (see the derivation of the determinant in the proof of Theorem 2), using fast algorithms for inversion of Vandermonde matrices such as [31] is more efficient than the explicit formula.

A difficulty with the inversion of $\mathbf{A}$ is that the resulting matrix for large N with a large variation in τ_n tends to be nearly singular (see the proof of Theorem 2). Moreover, it may not always be desirable to strictly limit the upper bandwidth because of the additional knowledge about the underlying process. A standard solution to address these problems simultaneously is to relax the constraints while penalizing the deviation from the ideal solution by a cost function. This technique is also known as Tikhonov regularization [32].

For a generic system of linear equations

$$\mathbf{A}\mathbf{x} = \mathbf{b},$$

a quadratic cost function can be defined as

$$C = \|\mathbf{A}\mathbf{x} - \mathbf{b}\|^2 + \|\mathbf{\Gamma}\mathbf{x}\|^2.$$

An explicit solution to this minimization problem is given by

$$\tilde{\mathbf{x}} = \left(\mathbf{A}^T\mathbf{A} + \mathbf{\Gamma}^T\mathbf{\Gamma}\right)^{-1}\mathbf{A}^T\mathbf{b}. \tag{16}$$

Based on the prior knowledge, a wide variety of matrices for $\mathbf{\Gamma}$ can be chosen. Note that this approach is equally applicable to (8) as well as (15). Furthermore, knowing that DFT and IDFT are expressible as matrices, one can convert the cost matrices between these two representations. We give a few examples for choosing $\mathbf{\Gamma}$ in the following subsections.

A. Time-Related Cost

Often, we are interested in interpolated signals that satisfy some smoothness criteria. To ensure this, one can minimize the difference between the values of two consecutive samples or minimize its variation across the samples. The former assumption favors constant signals and the latter means that the next sample should lie on the line extended from the two previous points. These assumptions resemble the behavior of Zero-Order Hold (ZOH) and First-Order Hold (FOH) signals between consecutive samples, respectively. Hence, we denote the associated $\mathbf{\Gamma}$ matrices by ZOH and FOH, such that

$$\mathbf{\Gamma}_{\text{ZOH}} = \begin{pmatrix} 1 & 0 & \cdots & 0 & -1 \\ -1 & 1 & \cdots & 0 & 0 \\ 0 & -1 & \cdots & 0 & 0 \\ \vdots & \vdots & \ddots & \ddots & \vdots \\ 0 & 0 & \cdots & -1 & 1 \end{pmatrix}, \tag{17}$$

$$\mathbf{\Gamma}_{\text{FOH}} = \mathbf{\Gamma}_{\text{ZOH}}\mathbf{\Gamma}_{\text{ZOH}}. \tag{18}$$

Finally, we substitute $\mathbf{\Gamma}$ with $\alpha\mathbf{\Gamma}_{\text{ZOH}}$ or $\alpha\mathbf{\Gamma}_{\text{FOH}}$ in (16).

B. Frequency-Related Cost

Although the proposed fitting approach inherently limits the frequency content, the time-related regularization tend to spread the spectrum. Thus, even if a lower bandwidth hypothesis for the underlying signal exists, we may not obtain it. This is evident in case of long drops because the algorithm, depending on the choice of $\mathbf{\Gamma}$, tends to find a constant or a piecewise linear solution in that range. One would run the algorithm in an iterative manner, i.e., after identifying the highest frequency from the spectrum of the first run, readjust T_s to achieve a lower bandwidth. Alternatively, this behavior can be controlled by introducing a cost for higher frequencies.

Several frequency-related cost formulations are possible. For example, using (15), the cost formulation for different scenarios is straightforward. Furthermore, we may use the fact that lower frequency signals could be represented by fewer samples over the same period. In other words, decreasing frequency corresponds to posing new constraints on $y[k]$ so that $\mathbf{0} = \mathbf{c}\tilde{\mathbf{y}}$ for some $\mathbf{c}$. These constraints can be calculated

using (8). We can form a non-square matrix that relates two sets of uniform samples at different sampling rates. By eliminating the variables corresponding to the lower sampling rate, the additional constraints can be found. Consequently, $\mathbf{\Gamma}$ in (16) can be set to $\alpha\mathbf{c}$. As a concrete example, we see that in case of down-sampling by a factor of two, every odd or even sample can be represented by the other set, which results in $N/2$ null constraints.

IV. Iterative Approach

The one-stage approach requires inverting a possibly large matrix. To circumvent this, a variety of iterative methods such as Richardson, Jacobi, and Gauss-Seidel [13] can be used. Instead of generic iterative methods, in this section we develop algorithms that take advantage of a non-integer delay element with respect to discrete-time signals.

Consider a signal evaluated at $t_n = (n+\tau)T_s$, $0 \le n < N$. Substituting τ_n with τ in (6) results in

$$\mathbf{y} = \mathbf{h}_\tau * \tilde{\mathbf{y}}_N, \tag{19}$$

where $*$ denotes the circular convolution and $\mathbf{h_\tau}$ is a sequence of length N taken from the periodic sinc function defined in (7),

$$h_\tau[n] = \mathrm{psinc}_N^\tau[n]\,. \tag{20}$$

Denoting the modolu operator by mod, $\tilde{y}_N[n] = \tilde{y}[n \bmod N]$.

The resulting signal $\mathbf{y}$ is a shifted version of the original signal with τT_s. Therefore, the operation can be interpreted as a non-integer forward shift element, where τ specifies the amount of shift as a fraction of the sampling period.

Now, we consider (19) in the frequency domain

$$\mathcal{F}\{\mathbf{y}\} = \mathcal{F}\{\mathbf{h}_\tau * \tilde{\mathbf{y}}_N\} \tag{21}$$

$$\Rightarrow \mathbf{Y} = \mathbf{H}^\tau \cdot \tilde{\mathbf{Y}}, \tag{22}$$

where $\mathcal{F}$ denotes the DFT and $\mathbf{Y}, \tilde{\mathbf{Y}}, \mathbf{H}^\tau \in \mathbb{C}^N$ are the results of the transformation. From the definition of the IDFT, we know that

$$h_\tau[n] = \frac{1}{N}\sum_{k=0}^{N-1} H_k^\tau \mathrm{e}^{i2\pi\frac{k}{N}n}, \qquad n = 0, \ldots, N-1. \tag{23}$$

Comparing (23) with (14), it is possible to find an explicit solution for $\mathbf{H}^\tau$. Namely,

$$H_k^\tau = \mathrm{e}^{i2\pi k\tau/N} \cdot \begin{cases} 1, & k = 0, \ldots, \lfloor\frac{N-1}{2}\rfloor \\ \mathrm{e}^{-i\pi\tau}\cos(\pi\tau), & k = \frac{N}{2} \qquad N \text{ even} \\ \mathrm{e}^{-i2\pi\tau}, & k = \lfloor\frac{N}{2}\rfloor + 1, \ldots, N-1. \end{cases} \tag{24}$$

Before we further discuss the interpolation technique, it is worth mentioning some of the properties of $\mathbf{H}^\tau$

$$\mathbf{H}^0 = 1 \tag{25}$$

$$H_k^1 = \mathrm{e}^{i2\pi k/N} \tag{26}$$

$$\mathbf{H}^{\tau *} = \mathbf{H}^{-\tau}, \tag{27}$$

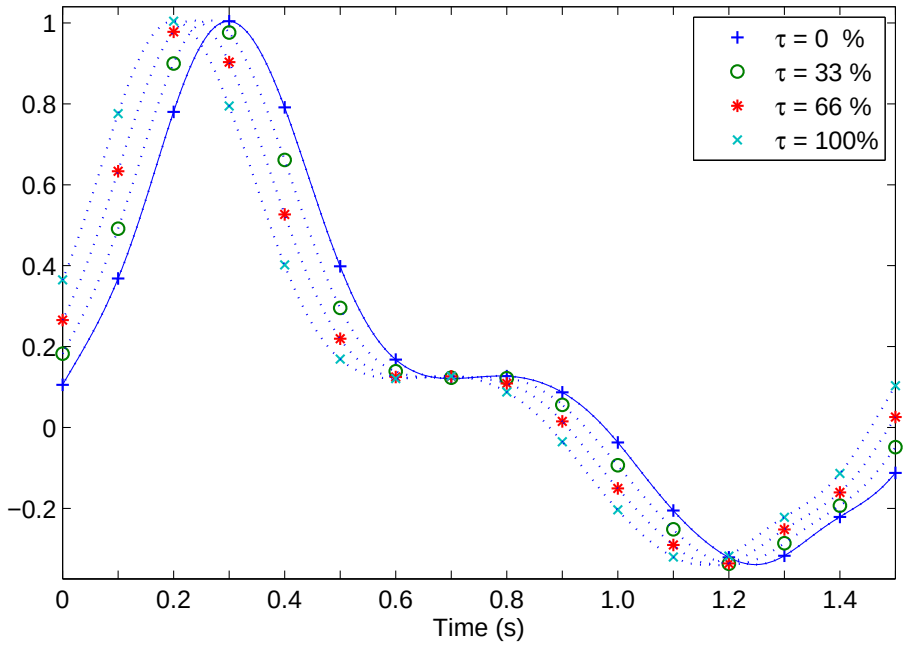

Fig. 1. Transformation of a signal by $\mathbf{H}^{\tau}$, where τ varies between 0-100%.

where the star denotes an element-wise complex conjugate. Furthermore, for $k \neq N/2$

$$H_k^{-\tau} = (H_k^{\tau})^{-1} \tag{28}$$

$$H_k^{\tau_1+\tau_2} = H_k^{\tau_1} \cdot H_k^{\tau_2}. \tag{29}$$

According to (24), $\mathbf{H}^{\tau}$ introduces phase shifts to each frequency component proportional to the frequency and the amount of τ. This is evidently a generalization of the delay element where (25) represents no shift and (26) is exactly the usual one sample forward shift. Figure 1 shows the transformation of a signal by $\mathbf{H}^{\tau}$ with several τ:s.

Let us introduce the following notation,

$$x_{\tau}[n] \equiv x\left(nT_s + \tau T_s\right). \tag{30}$$

Consequently, in the space of $\mathcal{B}_N$ we can write

$$\mathbf{X}_{\tau} = \mathbf{H}^{\tau} \cdot \mathbf{X}. \tag{31}$$

Proposition 1: If we assume $s \in \mathcal{B}_N$, and $\mathbf{x}$ are uniform samples of s, then $\forall N \in \mathbb{N}$ the effect of transformation by $\mathbf{h}_{\tau}$ is cumulative, i.e.,

$$\mathbf{x}_{\tau_1+\tau_2} = \mathbf{h}_{\tau_2} * \mathbf{x}_{\tau_1}. \tag{32}$$

Proof: We use (32) to write,

$$\mathbf{h}_{\tau_2} * \mathbf{x}_{\tau_1} = \mathcal{F}^{-1}\{\mathbf{H}^{\tau_2} \cdot \mathbf{H}^{\tau_1} \cdot \mathbf{X}\} \tag{33}$$

$$= \mathcal{F}^{-1}\{\mathbf{H}^{\tau_1+\tau_2} \cdot \mathbf{X}\} \tag{34}$$

$$= \mathbf{x}_{\tau_1+\tau_2}. \tag{35}$$

Since the space of $\mathcal{B}_N$ is strictly band-limited, $X_{N/2} = 0$ when N is even. To conclude (34), we have considered this fact and (29). ■

Corollary 2: The transformation by $\mathbf{H}^{\tau}$ is reversible.

Proof: Use $\tau_2 = -\tau_1 = -\tau$ in Proposition 1. Accordingly,

$$\mathbf{x}_{\tau} * \mathbf{h}_{-\tau} = \mathbf{x}_{\tau-\tau} = \mathbf{x}. \tag{36}$$

■

A. Sequential Mode Algorithm

Here, we present an algorithm based on the idea that each sample of $y(t_n)$ is a result of filtering the uniform samples, $y[k]$, with corresponding $\mathbf{H}^{\tau_n}$. Therefore, we can recover $y[k]$ by applying the inverse transform of these transformations. Since, the exact value of $y(kT_s + \tau_n T_s)$ is only known at $k = n$, we formulate an iterative algorithm to make use of this information:

1. $\tilde{\mathbf{y}} \leftarrow \mathbf{y}$ {Initialize}
2. **repeat**
3. **for all** $m \in \{0, \ldots, N-1\}$ **do**
4. $\tilde{\mathbf{y}}_{\tau_m} \leftarrow \mathcal{F}^{-1}\{\mathbf{H}^{\tau_m} \cdot \tilde{\mathbf{Y}}\}$
5. $\tilde{y}_{\tau_m}[m] \leftarrow y(t_m)$ {Correct sample m}
6. $\tilde{\mathbf{y}} \leftarrow \mathcal{F}^{-1}\{\mathbf{H}^{-\tau_m} \cdot \tilde{\mathbf{Y}}_{\tau_m}\}$
7. **end for**
8. **until** maximum iteration has reached **or** the remaining error is less than a desired value

In order to prove the convergence, we show that the energy of the error (sum of the squares of its elements) is constantly decreasing before the algorithm stops. The following Lemma proves that the energy of a signal transformed by $\mathbf{H}^{\tau}$ is equal to or less than the original signal. Provided that the signal is strictly band-limited, the energy is preserved.

Lemma 1: Let y_n denote the result of transforming signal x_n by $\mathbf{H}^{\tau}$, i.e., in the discrete Fourier domain $\mathbf{Y} = \mathbf{H}^{\tau} \cdot \mathbf{X}$, then

$$\sum_{n=0}^{N-1} |y_n|^2 \leq \sum_{n=0}^{N-1} |x_n|^2 . \tag{37}$$

Proof: We use Parseval's theorem to derive

$$\sum_{n=0}^{N-1} |y_n|^2 = \frac{1}{N} \sum_{k=0}^{N-1} |Y_k|^2 = \frac{1}{N} \sum_{k=0}^{N-1} |\mathbf{H}_k^{\tau} X_k|^2 \tag{38}$$

$$= \frac{1}{N} \sum_{k=0}^{N-1} \mathbf{H}_k^{\tau} \mathbf{H}_k^{\tau *} |X_k|^2 \tag{39}$$

$$\leq \frac{1}{N} \sum_{k=0}^{N-1} |X_k|^2 = \sum_{n=0}^{N-1} |x_n|^2 . \tag{40}$$

Equation (40) is concluded from (39) by using properties (27) and (28) and the fact that for $k = N/2$, $\mathbf{H}_k^{\tau} \mathbf{H}_k^{\tau *} = \cos^2(\pi\tau) \leq 1$. ■

Theorem 3: If the conditions of Theorem 2 hold, then the sequential mode algorithm converges to the solution of (8).

Proof: As a result of Theorem 2, there is a solution to (8), i.e., there is a $\tilde{\mathbf{y}}$ such that $\mathbf{y} = \mathbf{A}\tilde{\mathbf{y}}$. Accordingly, we can write the estimated samples at each iteration as the sum of the uniform samples of the reconstructed signal and an error

$$\tilde{\mathbf{y}}^{(k)} = \tilde{\mathbf{y}} + \mathbf{e}^{(k)}, \tag{41}$$

where superscript k denotes the iteration number.

Now, we show how the energy of the error in each step of the algorithm evolves. As a result of step 4,

$$\tilde{\mathbf{y}}^{(k)}_{\tau_m} = \left(\tilde{\mathbf{y}} + \mathbf{e}^{(k)}\right) * \mathbf{h}_{\tau_m}, \tag{42}$$

$$\tilde{\mathbf{y}}^{(k)}_{\tau_m} = \tilde{\mathbf{y}}_{\tau_m} + \mathbf{e}^{(k)}_{\tau_m}. \tag{43}$$

Step 5 results in

$$\tilde{\mathbf{y}}^{(k+1)}_{\tau_m} = \tilde{\mathbf{y}}_{\tau_m} + \mathbf{e}^{(k+1)}_{\tau_m}, \tag{44}$$

where

$$e^{(k+1)}_{\tau_m}[n] = \begin{cases} e^{(k)}_{\tau_m}[n], & n \neq m \\ 0, & n = m. \end{cases} \tag{45}$$

Assuming sample m is updated,

$$\sum_n \left|e^{(k+1)}_{\tau_m}[n]\right|^2 < \sum_n \left|e^{(k)}_{\tau_m}[n]\right|^2. \tag{46}$$

According to Corollary 2, we find

$$\tilde{\mathbf{y}}^{(k+1)} = \left(\tilde{\mathbf{y}}_{\tau_m} + \mathbf{e}^{(k+1)}_{\tau_m}\right) * \mathbf{h}_{-\tau_m} = \tilde{\mathbf{y}} + \mathbf{e}^{(k+1)}. \tag{47}$$

Using Lemma 1, (46) results in

$$\sum_n \left|\mathrm{e}^{(k+1)}[n]\right|^2 < \sum_n \left|\mathrm{e}^{(k)}[n]\right|^2. \tag{48}$$

This means that as long as a correction is made, the energy of the error is decreasing. Since the energy is bounded from below by zero, the algorithm will eventually converge to $\tilde{\mathbf{y}}$. ■

B. Batch Mode Algorithm

The sequential mode algorithm makes use of only one sample at each iteration and therefore its convergence rate is slow. To improve the situation, we try to make use of all samples in a batch fashion. The following algorithm shows the procedure:

1. $\tilde{\mathbf{y}} \leftarrow \mathbf{y}$ {Initialize}
2. **repeat**
3. $\quad \tilde{\mathcal{Y}}_\tau \leftarrow \mathcal{F}^{-1}\{\mathbb{H} \cdot \tilde{\mathbb{Y}}\}$
4. $\quad$ **for all** $m \in \{0, \ldots, N-1\}$ **do** {Replace the diagonal elements}
5. $\quad\quad \tilde{\mathcal{Y}}_\tau(m,m) \leftarrow \gamma y\left(t_m\right) + (1-\gamma)\tilde{\mathcal{Y}}_\tau(m,m)$
6. $\quad$ **end for**
7. $\quad \tilde{\mathcal{Y}} \leftarrow \mathcal{F}^{-1}\{\mathbb{H}^{-1} \cdot \tilde{\mathbb{Y}}_\tau\}$
8. $\quad \tilde{\mathbf{y}} \leftarrow \mathrm{diag}(\tilde{\mathcal{Y}})$ {Extract the diagonal}
9. **until** maximum iteration has reached **or** the remaining error is less than a desired value

Here, all the DFTs are row-wise and $\mathbb{H}, \tilde{\mathbb{Y}}, \tilde{\mathbb{Y}}_\tau \in \mathbb{C}^{N\times N}$ are defined as

$$\mathbb{H} = \begin{pmatrix} \mathbf{H}^{\tau_0} \\ \mathbf{H}^{\tau_1} \\ \vdots \\ \mathbf{H}^{\tau_{N-1}} \end{pmatrix}, \quad \tilde{\mathbb{Y}} = \begin{pmatrix} \tilde{\mathbf{Y}} \\ \tilde{\mathbf{Y}} \\ \vdots \\ \tilde{\mathbf{Y}} \end{pmatrix}, \quad \tilde{\mathbb{Y}}_\tau = \mathcal{F}\{\tilde{\mathcal{Y}}_\tau\}. \tag{49}$$

The relaxation parameter is in the interval $0 < \gamma \leq 1$.

Theorem 4: The following iterative algorithm describes a computationally more efficient counterpart to the batch mode algorithm,

$$\tilde{\mathbf{y}}^{(0)} = \mathbf{D}\mathbf{y} \tag{50}$$

$$\tilde{\mathbf{y}}^{(k+1)} = \tilde{\mathbf{y}}^{(k)} + \gamma\mathbf{D}\left(\mathbf{y} - \mathbf{A}\tilde{\mathbf{y}}^{(k)}\right), \tag{51}$$

where matrix $\mathbf{D}$ is a diagonal matrix that has the same diagonal elements as matrix $\mathbf{A}$.

Proof: We formulate the correction for the m-th sample at step 5 of the batch mode algorithm,

$$\Delta_{\tau_m}(n) = \gamma\left(y(t_m) - \tilde{y}^{(k)}_{\tau_m}[m]\right)\delta(n-m). \tag{52}$$

Accordingly,

$$\Delta(n) = \Delta_{\tau_m}(n) * h_{-\tau_m}[n] \tag{53}$$

$$= \gamma\left(y(t_m) - \tilde{y}^{(k)}_{\tau_m}[m]\right) h_{-\tau_m}[n-m]. \tag{54}$$

Now, if we evaluate (54) at m and build a new function out of its values, we obtain

$$\Delta'(m) = \gamma\left(y(t_m) - \tilde{y}^{(k)}_{\tau_m}[m]\right) h_{-\tau_m}[0]. \tag{55}$$

Therefore, a sample in the next iteration can be written in terms of the samples in the previous iteration as

$$\tilde{y}^{(k+1)}[n] = \tilde{y}^{(k)}[n] + \Delta'(n) \tag{56}$$

$$= \tilde{y}^{(k)}[n] + \gamma\left(y(t_n) - \tilde{y}^{(k)}_{\tau_n}[n]\right) h_{-\tau_n}[0]. \tag{57}$$

Writing (57) in a matrix form using the identities

$$\tilde{y}^{(k)}_{\tau_n}[n] = \sum_\ell \tilde{y}^{(k)}[\ell] h_{\tau_n}[n-\ell] \tag{58}$$

$$h_{\tau_n}[0] = h_{-\tau_n}[0], \tag{59}$$

completes the proof.

This reformulation is computationally beneficial since it scales with $O(N^2)$ instead of $O(N^2 \log N)$ at each iteration. ■

Corollary 3: The following algorithm recovers directly the spectral representation of non-uniformly sampled signals,

$$\tilde{\mathbf{Y}}^{(0)} = \mathcal{F}\{\mathbf{D}\mathbf{y}\} \tag{60}$$

$$\tilde{\mathbf{Y}}^{(k+1)} = \mathbf{T}\tilde{\mathbf{Y}}^{(k)} + \mathbf{C}, \tag{61}$$

where

$$\mathbf{T} = \mathbf{I} - \gamma\mathcal{F}\{\mathbf{D}\mathbf{W}\} \tag{62}$$

$$\mathbf{C} = \gamma\mathcal{F}\{\mathbf{D}\mathbf{y}\}, \tag{63}$$

and all the DFTs are column-wise.

Proof: This is the same as Theorem 4, expressed in the frequency domain using (15). ■

Note that in case of oversampled signals, using the formulation of Corollary 3 is beneficial. The reason is that we can remove the columns and rows corresponding to higher frequencies than the Nyquist frequency. Therefore, the computation in each iteration is reduced to $O(M^2)$, where M corresponds to the highest frequency in the discrete Fourier domain.

Lemma 2: Using the algorithm in Theorem 4, the error at each iteration evolves according to

$$\mathbf{e}^{(k)} = \mathbf{B}^k \mathbf{e}^{(0)}, \tag{64}$$

where

$$\mathbf{B} = \mathbf{I} - \gamma \mathbf{D}\mathbf{A}. \tag{65}$$

Proof: This is a direct consequence of (51). If we subtract both sides of (51) from the fixed point of the algorithm, it results in

$$\begin{aligned} \tilde{\mathbf{y}} - \tilde{\mathbf{y}}^{(k+1)} &= \tilde{\mathbf{y}} - \tilde{\mathbf{y}}^{(k)} - \gamma \mathbf{D}\left(\mathbf{y} - \mathbf{A}\tilde{\mathbf{y}}^{(k)}\right) \\ \mathbf{e}^{(k+1)} &= \mathbf{e}^{(k)} - \gamma \mathbf{D}\left(\mathbf{A}\tilde{\mathbf{y}} - \mathbf{A}\tilde{\mathbf{y}}^{(k)}\right) \\ \mathbf{e}^{(k+1)} &= \left(\mathbf{I} - \gamma \mathbf{D}\mathbf{A}\right)\mathbf{e}^{(k)}. \end{aligned} \tag{66}$$

By repeatedly applying (66), the proof is completed. ■

A necessary and sufficient condition for the convergence of the error to zero is that the spectral radius of matrix $\mathbf{B}$ is less than one, i.e., all the eigenvalues, denoted by λ_i, lie inside the unit circle

$$\rho(\mathbf{B}) = \max_i(|\lambda_i|) < 1. \tag{67}$$

Let us parametrize matrix $\mathbf{B}$ by $\boldsymbol{\tau} = (\tau_0, \tau_1, \ldots, \tau_{N-1})$. It is difficult to calculate an explicit solution to $\rho(\mathbf{B}_{\boldsymbol{\tau}})$ for a generic distribution of τ_n. However, we can show that for a given maximum deviation $\tau_{\max} = \max_n|\tau_n|$, $\boldsymbol{\tau} = \tau_{\max}\mathbf{1}_N$, i.e., $\tau_n = \tau_{\max}$ for $0 \le n < N$ is a local maximum of $\rho(\mathbf{B}_\tau)$. See Appendix B for the proof.

Theorem 5: Assuming $\rho(\mathbf{B}_{\boldsymbol{\tau}}) \le \lim_{N\to\infty} \rho(\mathbf{B}_{\tau_{\max}\mathbf{1}_N})$, the iterative algorithms of Theorem 4 and Corollary 3 are convergent in the range of $|\tau_n| < 1/2$ provided that

$$0 < \gamma \le \min\left(2/\mathrm{tanc}(\pi\tau_{\max}), 1\right),$$

where $\tau_{\max} = \max_{0\le n<N}|\tau_n|$ and $\mathrm{tanc}(x) = \tan(x)/x$.

Proof: See Appendix C. ■

Since according to Corollary 2 recovering a constant shift requires only one iteration, in order to utilize the fastest rate of convergence, we can remove the common offset of sampling instants before using the algorithms.

V. Results

In this section, we present different simulation scenarios to demonstrate the algorithms in practice. The scenarios cover the cases where there is only jitter or jitter and drops are both present. Since the cubic spline is commonly used for interpolation, we use it as a baseline for comparison. The iterative methods converge to the same solution as the one-stage method when there is no additional constraints. Therefore, we have not included any comparison between these two

approaches on the same data set. We use the normalized Mean-Squared Error (MSE) as the measure of accuracy. This is done according to

$$\mathrm{MSE} = \frac{\|\mathbf{y}_u - \tilde{\mathbf{y}}\|^2}{\|\mathbf{y}_u\|^2}, \tag{68}$$

where $\mathbf{y}_u$ denotes the uniform samples of the original signal.

A random complex spectrum with length $N = 128$ was used to build the test signals. We computed the time response by taking the IDFT. Thereafter, the signal was sampled non-uniformly. The jitter was a random function uniformly distributed in the range of $\pm 50\%$ of the sampling period.

In the first experiment, we used the one-stage method and filtered part of the spectrum by a notch filter. A sample signal is shown in Fig. 2.a and the spectra obtained without any preprocessing, using spline for interpolation and using the one-stage method are compared in Fig. 2.b. The one-stage approach provides solutions with an accuracy close to the machine precision.

Figures 3 and 4 correspond to a signal exploiting the whole spectrum recovered by means of Theorem 4 and Corollary 3, respectively. Figure 5 demonstrates the accuracy of the solution after each iteration of the batch mode algorithm (Theorem 4). The jitter was a random function uniformly distributed in the range of $\pm 15\%$, $\pm 30\%$, and $\pm 45\%$. No oversampling was used and $\gamma = 1$ in all experiments. For each range, the figure illustrates the results of one hundred experiments with different random signals and jitter profiles. The average MSE per iterations as well the worst and the best cases are shown.

In Table I, we present a numerical comparison between the batch mode algorithm and the cubic spline. We limited the jitter spread to $\pm 35\%$ and the maximum number of iterations to 10. Each row is characterized by a different M corresponding to the maximum frequency. The MSE values were averaged over one hundred experiments.

Table II shows the performance of the batch algorithm when some additive Gaussian measurement noise is present. The jitter spread was again set to $\pm 35\%$ and the maximum number of iterations to 10. For each row the standard deviation of the noise is $\sigma\|\mathbf{y}_u\|/N$. The MSE values were averaged over one hundred experiments.

In the drop scenarios, we limited the bandwidth to $M = 40$. The jitter was in the range of $\pm 35\%$ of the sampling period. We used the one-stage method with $\mathbf{\Gamma}_{\mathrm{ZOH}}$ and $\alpha = 0.001$. Figure 6.a shows a signal with a burst drop of length 5 while Fig. 6.b presents a scenario with recurrent drops at the rate of $0.3\,(\mathrm{drops/sample})$. Table III summarizes the results for various lengths of drops and rates of drops. The MSE values were averaged over one thousand experiments.

TABLE I
MSE OF THE BATCH MODE ALGORITHM AFTER 10 ITERATIONS COMPARED TO SPLINE

M	Batch Mode Alg. MSE (mean $\pm$ std)	Cubic Spline MSE (mean $\pm$ std)
63	$(1.04 \pm 1.28)\mathrm{e}{-6}$	$(4.78 \pm 2.09)\mathrm{e}{-2}$
48	$(8.42 \pm 15.9)\mathrm{e}{-7}$	$(6.20 \pm 4.27)\mathrm{e}{-3}$
32	$(3.00 \pm 4.24)\mathrm{e}{-7}$	$(2.49 \pm 1.45)\mathrm{e}{-4}$
16	$(1.19 \pm 1.96)\mathrm{e}{-7}$	$(9.49 \pm 6.85)\mathrm{e}{-7}$
4	$(1.06 \pm 1.26)\mathrm{e}{-8}$	$(2.68 \pm 2.24)\mathrm{e}{-11}$

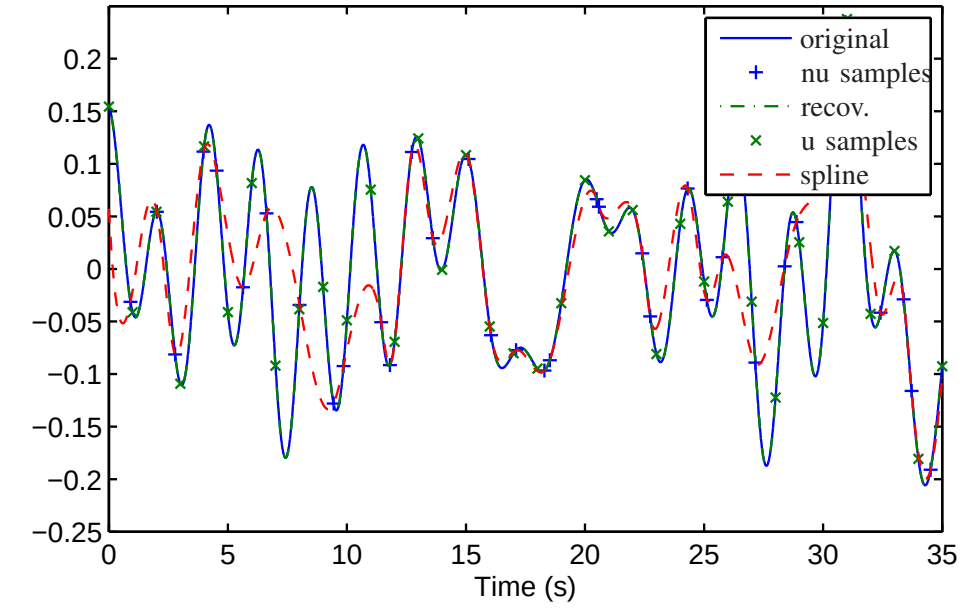

(a)

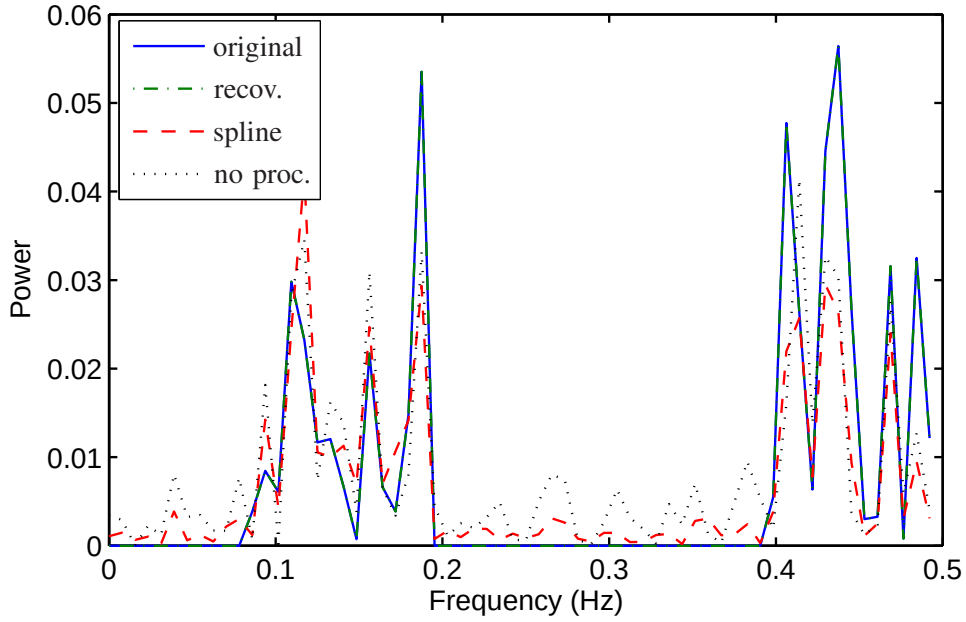

(b)

Fig. 2. Recovery of a signal by the one-stage approach (a) signals in the time domain and (b) the spectra. '+' denotes the non-uniform samples, solid line the original signal, 'x' the computed uniform samples, dash-dotted line the recovered signal, dashed line the interpolation by the cubic spline method, and dotted line no processing. Note that with no preprocessing or the spline method, erroneous frequency components are spread over the spectrum.

To give a better picture of the performance of the algorithms, we summarize a few observations here:

- With dense samples and relatively small weights there is no significant difference between $\mathbf{\Gamma}_{\mathrm{ZOH}}$ and $\mathbf{\Gamma}_{\mathrm{FOH}}$.
- For long drops, $\mathbf{\Gamma}_{\mathrm{FOH}}$ produces a similar result to spline, which is not desirable.
- Erroneous frequency components are usually scattered in the whole spectrum of a signal interpolated by the cubic spline method.

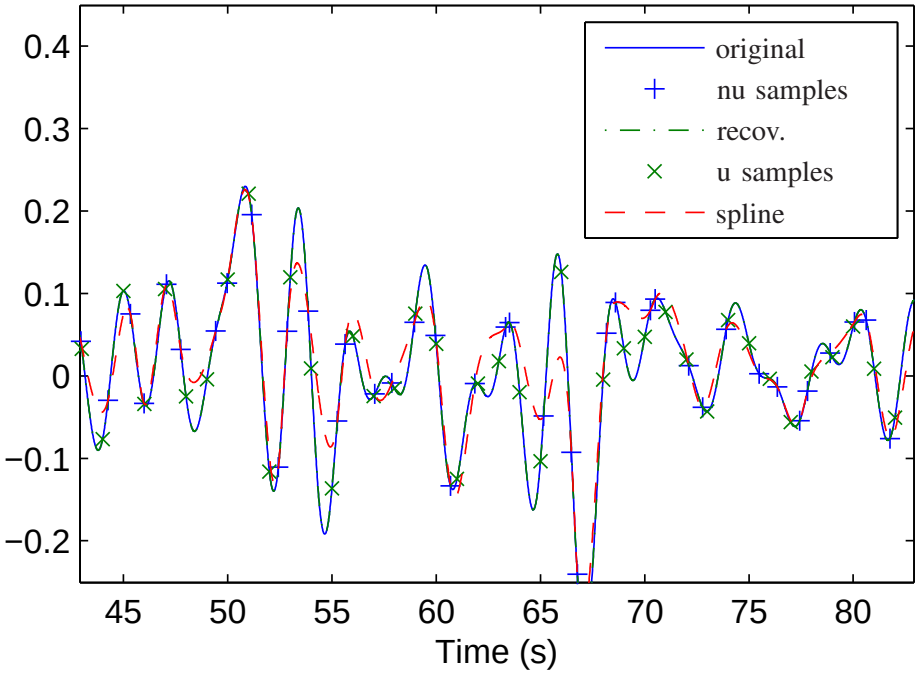

Fig. 3. Recovery of a signal by the batch mode algorithm (Theorem 4): '+' denotes the non-uniform samples, solid line the original signal, 'x' the computed uniform samples, dash-dotted line the recovered signal, and dashed line the interpolation by spline method.

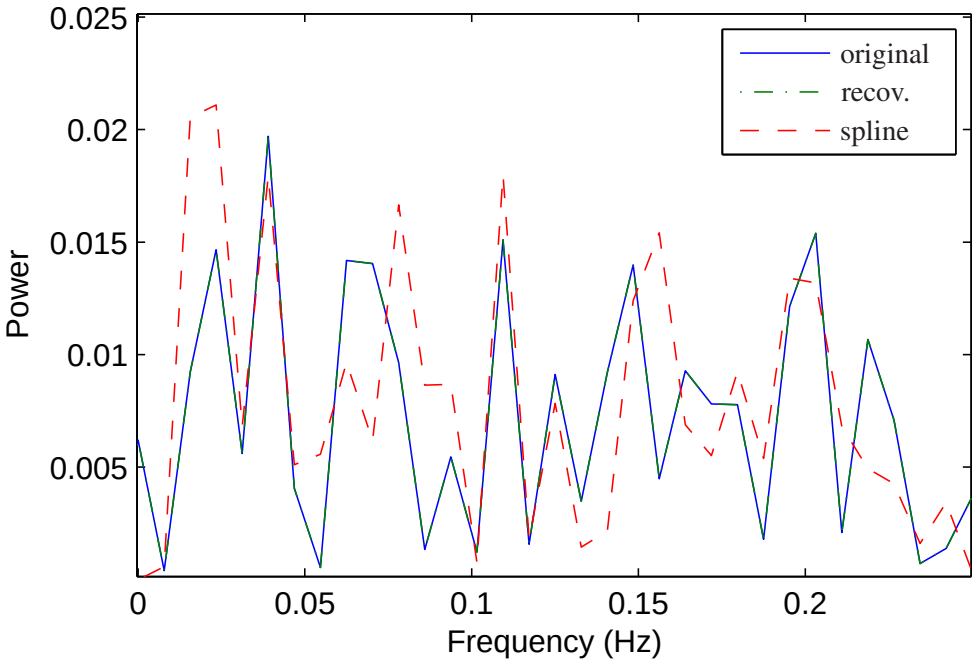

Fig. 4. Recovery of the spectrum by Corollary 3: solid line, dash-dotted line, and dashed line correspond to the original signal, recovered signal, and interpolation by the cubic spline method, respectively.

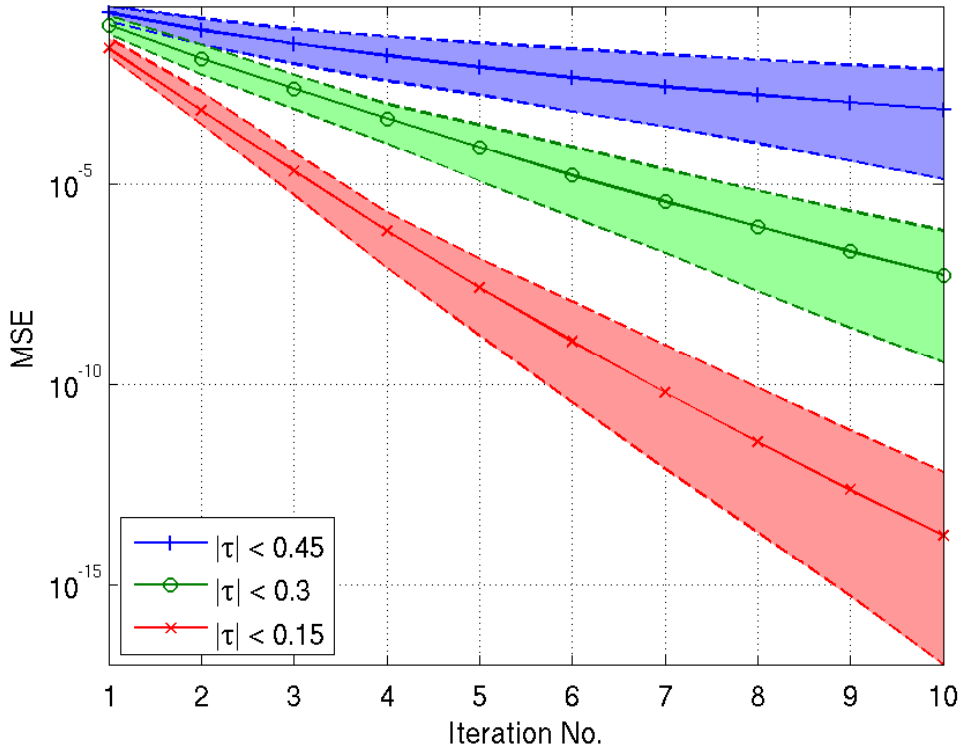

Fig. 5. Performance of the batch mode algorithm with respect to τ: The jitter is uniformly distributed in each given range. The solid lines correspond to the average over one hundred experiments for each range and the dashed lines correspond to the worst and the best scenarios.

- For larger N, the iterative methods reduce the error more quickly in the initial iterations. However, the length does not have a significant effect as the iterations proceed.
- Oversampling improves the performance of the algorithms as indicated in Table I. Additionally, the signals become more resilient to the loss of samples.
- Cubic spline performs well when signals are oversampled. However, with a higher frequency content our algorithms do significantly better. The spline interpolation totally fails in extrapolation and misses relatively rapid changes between two samples.
- For randomly distributed jitter, the condition number $\kappa(\mathbf{A})$ is small, which makes the algorithms robust to additive white noise.

TABLE II
RESULTS WITH ADDITIVE GAUSSIAN MEASUREMENT NOISE

σ	Batch Mode Alg. MSE (mean $\pm$ std)	Cubic Spline MSE (mean $\pm$ std)
0.01	$(1.49 \pm 0.84)\text{e} - 6$	$(5.09 \pm 2.05)\text{e} - 2$
0.02	$(4.21 \pm 3.19)\text{e} - 6$	$(5.24 \pm 2.08)\text{e} - 2$
0.05	$(2.07 \pm 0.29)\text{e} - 5$	$(5.34 \pm 2.67)\text{e} - 2$
0.1	$(7.91 \pm 0.93)\text{e} - 5$	$(5.06 \pm 1.94)\text{e} - 2$
0.2	$(3.09 \pm 0.33)\text{e} - 4$	$(5.00 \pm 2.09)\text{e} - 2$

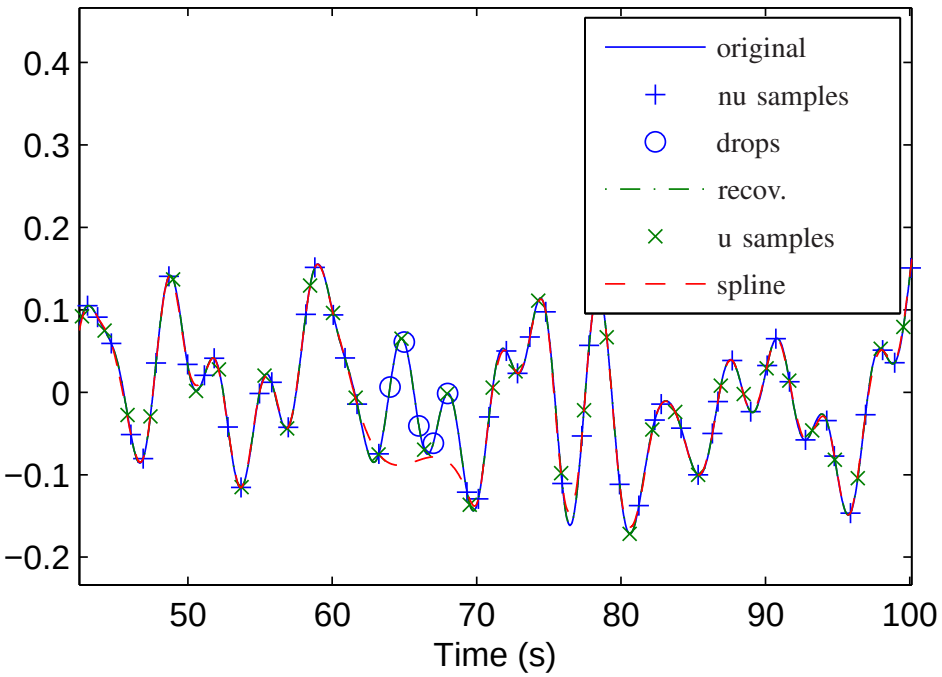

(a)

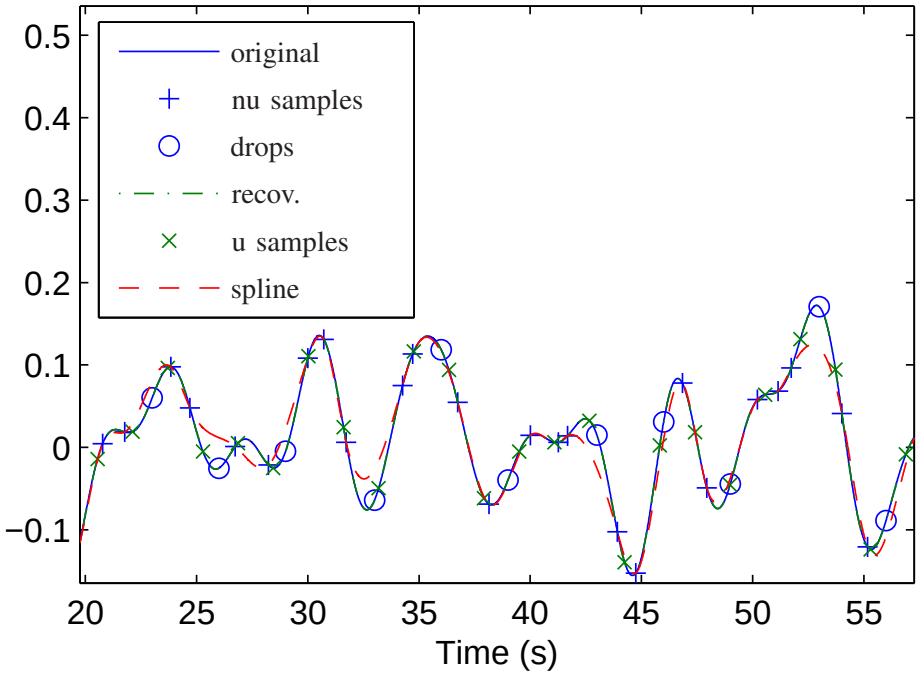

(b)

Fig. 6. Recovery of a signal with (a) burst drops and (b) recurrent drops: '+' denotes the non-uniform samples, circles the dropped samples, solid line the original signal, 'x' the computed uniform samples, dash-dotted line the recovered signal, and dashed line the interpolation by spline method. Note that the spline method misses rapid changes when the samples are dropped, while the one-stage method can recover them.

TABLE III
RESULTS OF ONE-STAGE APPROACH FOR BURST AND RECURRENT DROPS

Burst Drops

No.	Batch Mode Alg. MSE (mean $\pm$ std)	Cubic Spline MSE (mean $\pm$ std)
0	$(3.79 \pm 0.87)\text{e}{-5}$	$(1.32 \pm 0.90)\text{e}{-3}$
1	$(4.19 \pm 1.22)\text{e}{-5}$	$(2.51 \pm 2.22)\text{e}{-3}$
2	$(1.04 \pm 1.25)\text{e}{-4}$	$(1.42 \pm 1.84)\text{e}{-2}$
3	$(1.38 \pm 2.18)\text{e}{-3}$	$(4.57 \pm 5.81)\text{e}{-2}$
4	$(1.57 \pm 2.225)\text{e}{-2}$	$(7.85 \pm 8.64)\text{e}{-2}$
5	$(4.44 \pm 5.92)\text{e}{-2}$	$(9.54 \pm 9.65)\text{e}{-2}$

Recurrent Drops

Rate	Batch Mode Alg. MSE (mean $\pm$ std)	Cubic Spline MSE (mean $\pm$ std)
0	$(3.79 \pm 0.87)\text{e}{-5}$	$(1.32 \pm 0.90)\text{e}{-3}$
0.1	$(9.11 \pm 3.78)\text{e}{-5}$	$(1.56 \pm 0.76)\text{e}{-2}$
0.2	$(2.09 \pm 1.02)\text{e}{-4}$	$(3.15 \pm 1.26)\text{e}{-2}$
0.3	$(3.59 \pm 1.74)\text{e}{-4}$	$(6.22 \pm 2.50)\text{e}{-2}$
0.4	$(6.59 \pm 4.33)\text{e}{-2}$	$(4.86 \pm 5.43)\text{e}{-1}$
0.5	$(2.44 \pm 0.67)\text{e}{-1}$	$(4.88 \pm 3.45)\text{e}{-1}$

VI. DISCUSSION

As expected, our formulation leads to perfect reconstruction of the signals in the space of $\mathcal{B}_N$. In this case, our definition of digital fractional delay does not involve any approximation. Therefore, for periodic signals it is the counterpart of the perfect fractional delay defined in [33].

The periodic assumption has been explicitly or implicitly assumed in some other works, e.g., [17], [18], [24]. If this assumption is not valid, because of the decay rate of the $\text{sinc}(\cdot)$ function, reconstructed signals will have a more visible distortion at the boundaries compared to the middles. Therefore, signals with short intervals can suffer more while with an infinitely long period we expect no discrepancy according to (3). It is suggested that applying window functions on non-uniform samples can improve the performance [23]. Therefore, common windowing techniques [34] might be adopted for this purpose.

Theorem 2 implies that without the periodic assumption the solution is not unique. We may add homogeneous solutions, which are zero at the sampling points, to the recovered signal. Since any deviation from the periodic assumption appears as a perturbation of $\mathbf{y}$ in (8), the condition number $\kappa(\mathbf{A})$, plays an important role in the accuracy of the uniform samples in case of non-periodic signals.

Introducing minimum energy signals [12] is in fact another way to overcome non-uniqueness. However, under the assumption that a signal behaves similarly outside its measurement period, the periodic extension seems more appropriate. Moreover, as a common practice with the Fast Fourier Transform (FFT), the original signal can be padded with additional zeros or with mirrored data. Accordingly, the algorithms developed in this paper are able to accommodate a variety of methods to extend signals outside of their measurement window.

In the one-stage approach, the proposed methods for penalizing higher frequencies can be advantageous compared to low-pass filtering of the result since they

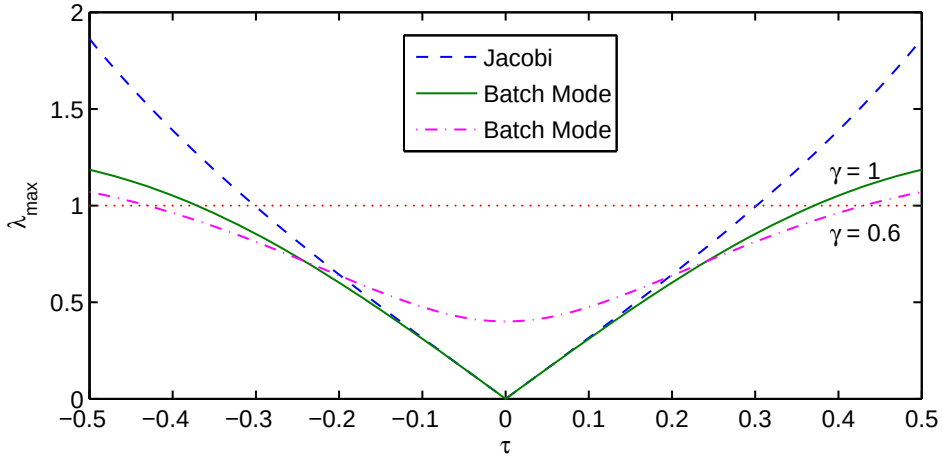

Fig. 7. Comparison of the convergence range of the Batch Mode algorithm and Jacobi iterative method for a constant offset. The batch mode algorithm remains convergent for a wider range of τ.

allow for a direct trade-off between the accuracy at the sampling instants and other desired properties. Assuming sparsity of the signals, it is possible to reconstruct them with less number of samples than the Nyquist rate [35]. This can for example be achieved by replacing the $\mathcal{L}_2$ norm of the signals in the one-stage approach with $\mathcal{L}_1$ norm and solving the resulting convex problem.

According to the results, the improvement in the spectrum by the methods proposed in this article is remarkable. Although the cubic spline improves the spectrum compared to the case of no-preprocessing, there are still spurious components both outside the frequency range and inside it. Therefore, a low-pass filter followed after the interpolation will not be able to fix the problem. Moreover, such a combination results in the loss of accuracy at the points where the interpolated signal is to pass through. On the contrary, in our approach we directly trade off between the accuracy and other smoothness criteria while keeping the bandwidth constant. Due to the strict enforcement of an upper frequency in case of no regularization, we do not expect that our algorithms do better than cubic spline for under-sampled signals.

To the authors' best knowledge, (2) and (24) have been stated in their most generic form while most authors consider a spectrum in $[-M, M]$, which implies that they restrict the analysis to odd numbers. For instance, our approach and in particular (2) provides a new insight to Corollary 3 of Theorem 1 in [18].

It is possible to compare the performance of the assumed worst case of our algorithm with the standard Jacobi iterative method (see [13] for the details of the Jacobi algorithm). Following the proof of Theorem 5, it is also possible to find $|\lambda_{\max}|$ for Jacobi method. Accordingly, we find the upper limit for convergence to be $|\tau_n| < \operatorname{sinc}^{-1}(0.5)/2 \approx 0.302$. This means that our algorithm converges in a wider range. Furthermore, Fig. 7 shows that in the same scenario by maintaining $\gamma = 1$, our algorithm has a better convergence property in the whole range. In practice, we observe that for uniformly distributed τ_n:s the situation is much better than the bound given in Theorem 5 and the algorithm remains convergent even without reducing γ.

It is worth mentioning that a fundamental difference between our approach and for example [24] and [12] is that instead of finding an explicit basis for the

expansion of a function based on its non-uniform samples, we reuse the uniform basis, but find new weights. The benefit with the latter approach is that it does not make the basis functions overcomplicated.

Note that by multiplying both sides of (15) by a certain matrix, our formulation becomes the same as the one in [22]. However, computing matrix $\mathbf{W}$ is more convenient than matrix $\mathbf{A}$ in [22]. Moreover, there is no requirement for pre-transformation of $\mathbf{y}$ in our approach.

If we similarly to Theorem 4 find out the equivalent form of the sequential mode algorithm, it is not difficult to verify that it is basically the POCS algorithm [20] for periodic signals where $\mathrm{sinc}(\cdot)$ function has been replaced by $\mathrm{psinc}(\cdot)$. This opens up the opportunity to bring in the strategies introduced in [21] for improving its convergence rate. Moreover, from this point of view, our batch mode algorithm is a generalization of the POCS algorithm in the sense that it tries to satisfy all the constraints at each iteration.

Here, we recite the condition of Theorem 1 in [16] for determining a signal by its non-uniform samples by means of their frame based algorithm

$$2M(2\lfloor d/2 \rfloor + 1) < N, \tag{69}$$

where d is the maximum distance between two samples and M is the bandwidth. Theorem 5 tells us that given a right relaxation parameter, the batch algorithm is convergent in the whole range $|\tau| < 1/2$. Reformulating this in terms of (69) and using the fact that oversampled signals can be resampled at a lower rate without loss of information, we obtain the following condition

$$d < 2N/(2M + 1). \tag{70}$$

From this perspective, our algorithm allows for larger d than Theorem 1 in [16] for $M < \lfloor (N-1)/2 \rfloor$.

VII. Conclusion

We have provided a formulation for recovering band-limited signals from a finite set of irregularly sampled data. One-stage and iterative methods have been proposed that allow us to recover signals either in the time domain or the frequency domain. In our approach, non-uniform samples specify constraints on the recovered signals. This framework enables us to introduce easily a variety of additional constraints. For instance, one might wish to filter out a certain frequency range or fill in the missing data.

An integral ingredient for the design of our iterative methods is the notion of a discrete-time non-integer delay element. The delay element, which is a generalization of a one-sample shift operator, is inspired by the frequency view of our formulation. Thanks to this delay element, the iterative methods can shift signals in time and satisfy the constraints imposed by non-uniform samples step by step.

Both iterative and one-stage approaches solve the same problem and without additional considerations provide the same solution. Whereas it is easier to incorporate additional constraints in the one-stage algorithm, the iterative methods do no need to carry out computationally demanding operations such as matrix inversion. Moreover, the iterative methods are able to handle a large variation in the sampling instants (up to $\pm 50\%$ jitter). Therefore, they scale up better for longer measurement sequences.

In accordance with our initial motivation, these algorithms can constitute an effective preprocessing stage in system identification. Nonetheless, the application

is not limited to this area and they might as well be considered in other areas such as image processing or asynchronous transmission.

ACKNOWLEDGEMENT

The authors would like to thank for feedback and comments on the manuscript of this article from their colleagues at the Department of Automatic Control at Lund University.

APPENDIX A
PROOF OF THEOREM 2

In order for a square matrix to have full rank, it is sufficient that its determinant and hence its factors be non-zero. According to Theorem 1, $\mathbf{A} = \mathbf{WV}$. Therefore,

$$\det(\mathbf{A}) = \det(\mathbf{W}) \det(\mathbf{V}). \tag{71}$$

Matrix $\mathbf{V}$ is a Vandermonde matrix and hence its determinant is

$$\det(\mathbf{V}) = \prod_{0 \le i < j < N} (v_j - v_i)\,. \tag{72}$$

It is also possible to derive the determinant of $\mathbf{W}$ based on the determinant of a standard Vandermonde matrix. Let us define a diagonal matrix such that

$$D_{nn} = w_n^{\lfloor \frac{N}{2} \rfloor}. \tag{73}$$

If N is odd, $\mathbf{W}' = N\mathbf{DW}$ is a Vandermonde matrix with permuted columns. Since it has an even parity permutation, its determinant is equal to an ordinary Vandermonde matrix. The determinant of $\mathbf{D}$ is simply the product of its diagonal elements. Therefore, we conclude

$$\det(\mathbf{W}) = \frac{1}{N^N} \frac{\det(\mathbf{W}')}{\det(\mathbf{D})}. \tag{74}$$

Similarly, we can define $\mathbf{W}'$ when N is even. Thereafter, we build two matrices $\mathbf{W}'_1$ and $\mathbf{W}'_2$ equal to $\mathbf{W}'$, except their $N/2$-th column should sum up to the $N/2$-th column of $\mathbf{W}'$. Using the n-linear function property of determinants, we find

$$\det(\mathbf{W}') = \frac{1}{2} \det(\mathbf{W}'_1) + \frac{1}{2} \det(\mathbf{W}'_2). \tag{75}$$

By choosing the $N/2$-th column of $\mathbf{W}'_1$ to be a constant vector with its all elements equal to $1/2$, $\mathbf{W}'_1$ becomes a Vandermonde matrix with permuted columns. We multiply $\mathbf{W}'_2$ from the left by $\mathbf{D}'$ to obtain another Vandermode matrix

$$\mathbf{W}'' = \mathbf{D}'\mathbf{W}'_2, \tag{76}$$

where $D'_{nn} = w_n^{-1}$. Putting all these together, we conclude

$$\det(\mathbf{W}) = \begin{cases} \overbrace{\dfrac{1}{N^N} \displaystyle\prod_{0 \le k < N} w_k^{-p} \prod_{0 \le i < j < N} (w_j - w_i)}^{E}, & N \text{ odd} \\ \dfrac{(-1)^p}{2} \left(1 - \displaystyle\prod_{0 \le k < N} w_k\right) E, & N \text{ even}, \end{cases} \tag{77}$$

where $p = \lfloor N/2 \rfloor$.

Obviously, the factors of $\det(\mathbf{V})$ are non-zero. We observe that if t_n are distinct for all $n \in \{0, \ldots, N-1\}$, w_n:s are also different. Regarding the case where N is even, the following relation holds

$$\prod_{0 \le k < N} w_k = 1 \angle \phi, \tag{78}$$

where

$$\begin{aligned}
\phi &= \sum_{n=0}^{N-1} \frac{2\pi}{N} (n + \tau_n) + 2k\pi \\
&= \frac{2\pi}{N} \left(\sum_{n=0}^{N-1} \tau_n + N(N-1)/2 \right) + 2k\pi \\
&= \frac{2\pi}{N} \sum_{n=0}^{N-1} \tau_n + \pi(N-1) + 2k\pi \\
&= \frac{2\pi}{N} \sum_{n=0}^{N-1} \tau_n - \pi + 2k'\pi.
\end{aligned} \tag{79}$$

In (79), we have defined $k' = k + N/2$. Setting $\phi \neq 2k\pi$ results in

$$\sum_{n=0}^{N-1} \tau_n \neq (2k+1)N/2, \ k \in \mathbb{Z}. \tag{80}$$

Let us assume $|\tau_n| < 1/2$. It follows that

$$\left| \sum_{n=0}^{N-1} \tau_n \right| < N/2. \tag{81}$$

This implies $(2k'-1)\pi < \phi < 2k'\pi$ and hence the last factor cannot be zero. This proves the corollary. ■

Appendix B
Spectral Radius of $\mathbf{B}_{\boldsymbol{\tau}}$

Due to the symmetry of the problem, the eigenvalues of $\mathbf{B}_{\boldsymbol{\tau}}$ is invariant to any number of the circular shift of $\boldsymbol{\tau}$. Additionally, flipping and negating $\boldsymbol{\tau}$ does not change the eigenvalues. Now, we consider the gradient of the spectral radius with respect to vector $\boldsymbol{\tau}$. Using the first property, we conclude,

$$\begin{aligned}
\nabla\rho(\tau_0, \tau_1, \ldots, \tau_{N-1}) &= \frac{\partial\rho}{\partial\tau_0}\hat{i} + \frac{\partial\rho}{\partial\tau_1}\hat{j} + \ldots \Big|_{(\tau_0, \tau_1, \ldots, \tau_{N-1})} \\
&= \frac{\partial\rho}{\partial\tau_1}\hat{i} + \frac{\partial\rho}{\partial\tau_2}\hat{j} + \ldots \Big|_{(\tau_1, \ldots, \tau_{N-1}, \tau_0)} \\
&= \ldots \\
&= \frac{\partial\rho}{\partial\tau_{N-1}}\hat{i} + \frac{\partial\rho}{\partial\tau_0}\hat{j} + \ldots \Big|_{(\tau_{N-1}, \tau_0, \ldots, \tau_{N-2})}
\end{aligned}$$

Now assuming $\boldsymbol{\tau} = c\mathbf{1}_N$, i.e., $\tau_n = c$ for $0 \le n < N$, the circular shift results in the same vector. Therefore, on the line $\tau_n = c > 0$ we have

$$\frac{\partial\rho}{\partial\tau_0} = \frac{\partial\rho}{\partial\tau_1} = \cdots = \frac{\partial\rho}{\partial\tau_{N-1}}.$$

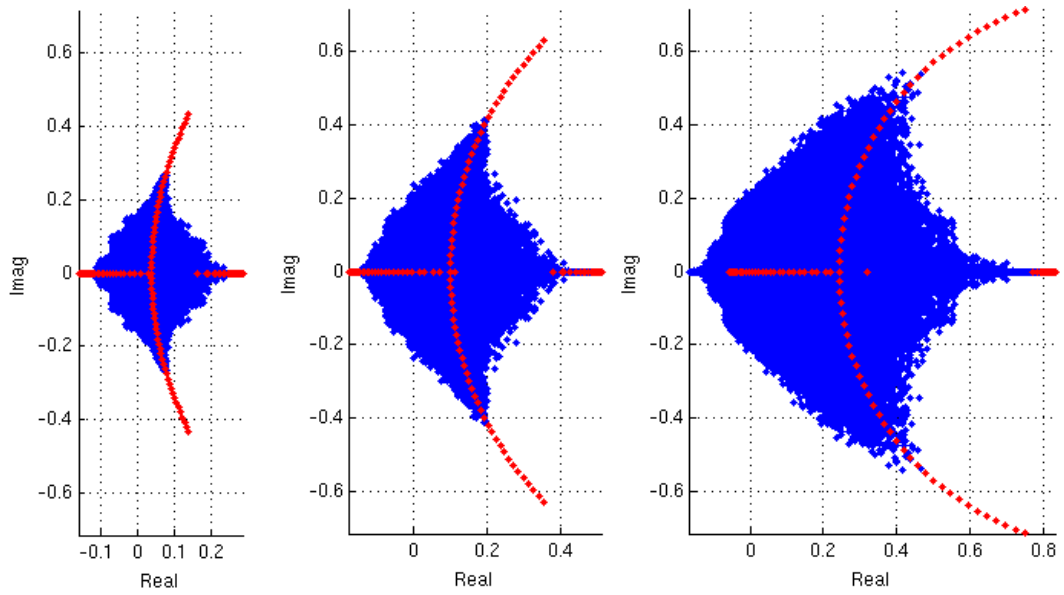

Fig. 8. Eigenvalue of matrix $\mathbf{B}_{\boldsymbol{\tau}}$: In the left figure, the vertical arc corresponds to $\tau_n = 0.15$ for $0 \leq n < 65$, the horizontal line to $\tau_n = (-1)^n 0.15$, and the rest of the dots show the overlaid eigenvalues of randomly generated matrices with $\tau_{\max} = 0.15$. The other figures are generated similarly. The figure in the middle and to the right correspond to $\tau_{\max} = 0.25$ and $\tau_{\max} = 0.4$, respectively.

This implies that starting from any point on this line and following the steepest ascend direction, we will not leave the line. Since the spectral radius increases as c increases (see (87) in Appendix C), we conclude that $\boldsymbol{\tau} = \tau_{\max}\mathbf{1}_N$ is in fact a local maximum.

Fig. 8 illustrates several examples of the distribution of the eigenvalues for $N = 65$. The blue dots correspond to the eigenvalues of many randomly generated matrices $\mathbf{B}_{\boldsymbol{\tau}}$ for a given $\tau_{\max}$. The horizontal line and the vertical arc show the eigenvalues corresponding to $\tau_n = (-1)^n \tau_{\max}$ and $\tau_n = \tau_{\max}$, respectively. Note that the spectral radius is determined by the point that lies farthest away from the origin.

Appendix C
Proof of Theorem 5

According to the definition of $\mathbf{B}$ in (65), we can write

$$\det(\mathbf{B} - \lambda\mathbf{I}) = 0 \Rightarrow \tag{82}$$

$$\det(\gamma\mathbf{DA} - (1-\lambda)\mathbf{I}) = 0. \tag{83}$$

Therefore, the eigenvalues of matrix $\mathbf{B}$ are related to $\mathbf{DA}$ through

$$\lambda(\mathbf{B}) = 1 - \gamma\lambda(\mathbf{DA}). \tag{84}$$

For $\tau_n = \tau = \tau_{\max}$, matrix $\mathbf{DA}$ becomes circulant. The eigenvalues of a circulant matrix are equal to the DFT of any of its columns. We observe that the first column of $\mathbf{DA}$ is equal to $(DA)_{n,1} = h_\tau[0]h_\tau[n]$. Consequently, the eigenvalues are calculated as

$$\lambda_n = 1 - \gamma\mathcal{F}\{h_\tau[0]h_\tau[n]\} \tag{85}$$

$$= 1 - \gamma h_\tau[0]H_n^\tau, \tag{86}$$

and

$$\rho(\mathbf{B}) = \max_n |1 - \gamma h_\tau[0] H_n^\tau|. \tag{87}$$

From (24), we can verify that the maximum is obtained around $N/2$, corresponding to high frequencies. In addition, as the number of samples tends to infinity the spectral radius increases. Therefore,

$$\rho(\mathbf{B}) < \lim_{N\to\infty} |1 - \gamma h_\tau[0] H_n^\tau|, \tag{88}$$

where $n \in \left\{ \lfloor \frac{N-1}{2} \rfloor, \lfloor \frac{N}{2} \rfloor + 1 \right\}$. This results in

$$\rho(\mathbf{B}) < \sqrt{1 + \gamma^2 \mathrm{sinc}^2(\tau) - 2\gamma \cos(\pi\tau)\mathrm{sinc}(\tau)}. \tag{89}$$

The theorem is proved by equating the right hand side of (89) to one and solving for γ. This provides us with an upper bound for γ. ■

REFERENCES

[1] M. Unser, "Sampling-50 years after Shannon," *Proc. IEEE*, vol. 88, no. 4, pp. 569–587, Apr. 2000.

[2] I. Bilinskis and A. Mikelsons, *Randomized signal processing*. New York: Prentice Hall, 1992.

[3] F. Papenfuss, Y. Artyukh, E. Boole, and D. Timmermann, "Optimal sampling functions in nonuniform sampling driver designs to overcome the Nyquist limit," in *Proc. IEEE Int. Conf. Acoustics, Speech, and Signal Processing (ICASSP '03)*, vol. 6, Hong Kong, Apr. 2003, pp. 257–60.

[4] V. Singh and N. Rajpal, "Data compression using non-uniform sampling," in *Proc. IEEE Int. Conf. Signal Processing, Communications and Networking (ICSCN '07)*, Chennai, India, Feb. 2007, pp. 603–607.

[5] C. De Boor, *A practical guide to splines*. New York: Springer-Verlag, 1978.

[6] Y. Lyubarskii and W. Madych, "The recovery of irregularly sampled band limited functions via tempered splines," *J. Functional Analysis*, vol. 125, no. 1, pp. 201–222, 1994.

[7] R. E. A. C. Paley and N. Wiener, *Fourier transforms in the complex domain*, ser. American Mathematical Society Colloquium Publications. Providence, RI: American Mathematical Society, 1987, vol. 19, reprint of the 1934 original.

[8] M. Kadec, "The exact value of the Paley-Wiener constant," *Sov. Math. Doklady*, vol. 5, no. 2, pp. 559–561, 1964.

[9] A. Beurling and L. Carleson, *The Collected Works of Arne Beurling: Harmonic analysis*, ser. Contemporary mathematicians. Boston: Birkhäuser, 1989.

[10] H. Landau, "Necessary density conditions for sampling and interpolation of certain entire functions," *Acta Mathematica*, vol. 117, pp. 37–52, 1967.

[11] R. J. Duffin and A. C. Schaeffer, "A class of nonharmonic Fourier series," *Trans. American Mathematical Society*, vol. 72, no. 2, pp. 341–366, 1952.

[12] J. Yen, "On nonuniform sampling of bandwidth-limited signals," *IRE Trans. Circuit Theory*, vol. 3, no. 4, pp. 251–257, Dec. 1956.

[13] L. A. Hageman and D. M. Young, *Applied Iterative Methods*. New York: Academic Press, 1981.

[14] F. Marvasti, M. Analoui, and M. Gamshadzahi, "Recovery of signals from nonuniform samples using iterative methods," *IEEE Trans. Signal Process.*, vol. 39, no. 4, pp. 872–878, 1991.

[15] F. Marvasti, Ed., *Nonuniform Sampling: Theory and Practice*. New York: Kluwer, 2000.

[16] K. Gröchenig, "A discrete theory of irregular sampling," *Linear Algebra and its Applications*, vol. 193, pp. 129–150, 1993.

[17] H. G. Feichtinger, K. Gröchenig, and T. Strohmer, "Efficient numerical methods in non-uniform sampling theory," *Numerische Mathematik*, vol. 69, pp. 423–440, 1995.

[18] K. Gröchenig, "Irregular sampling, Toeplitz matrices, and the approximation of entire functions of exponential type," *Mathematics of Computation*, vol. 68, no. 226, pp. 749–765, 1999.

[19] A. Aldroubi and K. Gröchenig, "Nonuniform sampling and reconstruction in shift-invariant spaces," *SIAM Review*, vol. 43, no. 4, pp. 585–620, 2001.

[20] S. Yeh and H. Stark, "Iterative and one-step reconstruction from nonuniform samples by convex projections," *J. Optical Society of America*, vol. 7, no. 3, pp. 491–499, Mar. 1990.

[21] H. G. Feichtinger, C. Cenker, M. Mayer, H. Steier, and T. Strohmer, "New variants of the POCS method using affine subspaces of finite codimension with applications to irregular sampling," in *Applications in Optical Science and Engineering*. Int. Society for Optics and Photonics, 1992, pp. 299–310.

[22] Y. Jenq, "Perfect reconstruction of digital spectrum from nonuniformly sampled signals," *IEEE Trans. Instrum. Meas.*, vol. 46, no. 3, pp. 649–652, 1997.

[23] T. E. Tuncer, "Block-based methods for the reconstruction of finite-length signals from nonuniform samples," *IEEE Trans. Signal Processing*, vol. 55, no. 2, pp. 530–541, Feb. 2007.

[24] E. Margolis and Y. Eldar, "Nonuniform sampling of periodic bandlimited signals," *IEEE Trans. Signal Processing*, vol. 56, no. 7, pp. 2728–2745, Jul. 2008.
[25] C. Shannon, "Communication in the presence of noise," in *Proc. IRE*, vol. 37, no. 1, Jan. 1949, pp. 10–21.
[26] A. Jerri, "The Shannon sampling theorem—Its various extensions and applications: A tutorial review," *Proc. IEEE*, vol. 65, no. 11, pp. 1565–1596, Nov. 1977.
[27] T. Glad and L. Ljung, *Control Theory: Multivariable & Nonlinear Methods*. London: Taylor & Francis, Mar. 2000.
[28] E. T. Whittaker, "On the functions which are represented by the expansions of the interpolation theory," in *Proc. Royal Society of Edinburgh*, vol. 35, 1915, pp. 181–194.
[29] T. Cavicchi, "DFT time-domain interpolation," in *IEE Proc. F - Radar and Signal Processing*, vol. 139, no. 3, Jun 1992, pp. 207–211.
[30] S. Dooley and A. Nandi, "Notes on the interpolation of discrete periodic signals using sinc function related approaches," *IEEE Trans. Signal Processing*, vol. 48, no. 4, pp. 1201–1203, Apr 2000.
[31] I. Gohberg and V. Olshevsky, "The fast generalized Parker-Traub algorithm for inversion of Vandermonde and related matrices," *Journal of Complexity*, vol. 13, no. 2, pp. 208–234, 1997.
[32] A. N. Tichonov and V. J. Arsenin, *Solutions of ill-posed problems*, F. John, Ed. New York: V.H. Winston and Sons; Wiley, 1977.
[33] T. Laakso, V. Valimaki, M. Karjalainen, and U. Laine, "Splitting the unit delay [FIR/all pass filters design]," *IEEE Signal Processing Magazine*, vol. 13, no. 1, pp. 30–60, Jan. 1996.
[34] R. Johansson, *Predictive and adaptive control*. Lund, Sweden: Dept. Automatic Control, Lund University, 2009.
[35] E. J. Candès, J. Romberg, and T. Tao, "Robust uncertainty principles: Exact signal reconstruction from highly incomplete frequency information," *IEEE Trans. Information Theory*, vol. 52, no. 2, pp. 489–509, 2006.